JACS
JOURNAL OF THE AMERICAN CHEMICAL SOCIETY

Communication

pubs.acs.org/JACS

# Prototypes of Lanthanide(III) Agents Responsive to Enzymatic Activities in Three Complementary Imaging Modalities: Visible/Near-Infrared Luminescence, PARACEST-, and $T_1$-MRI

Jiefang He,[†] Célia S. Bonnet,[‡] Svetlana V. Eliseeva,[‡] Sara Lacerda,[‡] Thomas Chauvin,[‡] Pascal Retailleau,[†] Frederic Szeremeta,[‡] Bernard Badet,[†] Stéphane Petoud,*[,‡] Éva Tóth,*[,‡] and Philippe Durand*[,†]

[†]Institut de Chimie des Substances Naturelles, CNRS UPR 2301, Université Paris-Saclay, 1, av.de la Terrasse, 91198 Gif-sur-Yvette, France

[‡]Centre de Biophysique Moléculaire, CNRS UPR 4301, Université d'Orléans, Rue Charles Sadron, F-45071 Orléans 2, France

Supporting Information

**ABSTRACT:** We report first prototypes of responsive lanthanide(III) complexes that can be monitored independently in three complementary imaging modalities. Through the appropriate choice of lanthanide(III) cations, the same reactive ligand can be used to form complexes providing detection by (i) visible ($Tb^{3+}$) and near-infrared ($Yb^{3+}$) luminescence, (ii) PARACEST- ($Tb^{3+}$, $Yb^{3+}$), or (iii) $T_1$-weighted ($Gd^{3+}$) MRI. The use of lanthanide(III) ions of different natures for these imaging modalities induces only a minor change in the structure of complexes that are therefore expected to have a single biodistribution and cytotoxicity.

Molecular imaging aims at visualizing biological objects or biochemical events at physiological, cellular, and molecular levels within living cells, tissues or whole organisms for research, diagnostics, or personalized medicine purposes.[1] It relies on selective and/or responsive imaging agents optimized for a specific imaging modality,[2] i.e., magnetic resonance imaging (MRI),[3] optical imaging,[4] ultrasonography,[5] tomography,[6] etc. As each modality has its advantages and limitations, additional and less ambiguous information becomes accessible by sequentially or simultaneously combining several complementary techniques.[7] The broad diversity of molecular events requires innovative solutions for their monitoring. Among them, enzymatic activities are of interest since their dysregulation is involved in many diseases. Smart imaging agents endowed with a responsive mechanism are required to detect these activities.[8] Despite long-term efforts, progress in *in vivo* responsive imaging remains limited.[9] An appealing strategy to accelerate the development of molecular imaging relies in the design of responsive probes suitable for different detection techniques using versatile molecular platforms, thus optimizing both time and efforts for synthetic work. Such platforms must combine a trigger, which can be adapted to a broad variety of molecular events, and a reporter moiety that can be detected by several imaging modalities.[10] We previously designed a platform suitable for detection of enzymatic activities by PARACEST-MRI[11] in which an enzyme-specific trigger was coupled to a $Ln^{3+}$-based reporter using a self-immolative spacer. We have demonstrated that the action of the selected enzyme resulted in elimination of the spacer associated with a change in MRI signal. In the present work, we set the basis of smart imaging probes, which, in addition to PARACEST-MRI, allow the detection of enzymatic event by visible and near-infrared (NIR) luminescence and by $T_1$-MRI. Bioimaging in the NIR provides a major advantage of enhanced detection sensitivity due to the limited autofluorescence of biological tissues in this energy window.[12] Several NIR-emitting $Ln^{3+}$ ions[13] proved attractive for microscopy imaging of living cells.[14] Moreover, $Ln^{3+}$-based imaging agents possess several complementary advantages over organic fluorophores, such as sharp emission bands (for spectral discrimination) and strong resistance to photobleaching.[15]

As $Ln^{3+}$ cations possess versatile magnetic and optical properties while having similar reactivities,[16] we have designed a molecular platform that can be made responsive and that is compatible with the complementary imaging modalities previously described (Scheme 1). Ligand $\mathbf{H_3L_1}$ is a DO3A derivative substituted by a pyridylmethyl moiety. The pyridine has multiple roles here: (i) to provide a donor atom for stable $Ln^{3+}$ complexation,[17] (ii) to act as a sensitizer for $Ln^{3+}$

**Scheme 1. $Ln^{3+}$ Complexes as Prototypes of Enzyme Responsive Probes for Detection by Visible ($Tb^{3+}$) or Near-Infrared ($Yb^{3+}$) Luminescence, by $T_1$-Weighted- ($Gd^{3+}$), or by PARACEST- ($Yb^{3+}$, $Tb^{3+}$) MRI[a]**

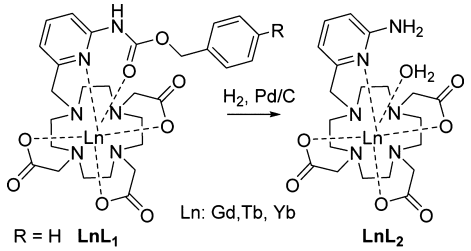


[a]The R in $\mathbf{LnL_1}$ can be replaced by an appropriate substrate to afford enzyme sensitivity and specificity.

**Received:** November 23, 2015
**Published:** January 4, 2016





DOI: 10.1021/jacs.5b12084
J. Am. Chem. Soc. 2016, 138, 2913−2916

luminescence (antenna effect),[18] and (iii) to introduce additional functionalities, in particular a self-immolative benzyl carbamate that will make this reporter responsive to molecular events such as enzymatic cleavage, as previously reported.[11] The enzymatic cleavage of such probe and the elimination of the self-immolative arm will induce the transformation of the carbamate into an amine[19] with subsequent changes in the coordination environment of the $Ln^{3+}$ ion and modification of its hydration state. We hypothesized that such switching would be detectable by both visible and NIR luminescence as well as by $T_1$- and PARACEST-MRI depending on the nature of the $Ln^{3+}$. We note that PARACEST and $T_1$ agents cannot be used simultaneously since the $T_1$ agent destroys the CEST signal; however, sequential imaging of the same animal in the two techniques can ascertain the findings and provide more accurate information. The luminescence capability provides higher sensitivity and resolution at the cellular level giving complementary information. $\mathbf{LnL_1}$ are synthetically accessible model complexes of the responsive probes that will bear the self-immolative benzyl carbamate linker and an enzyme-specific substrate (R). For instance, $\beta$-D-galactopyranoside can be used as a substrate for the detection of $\beta$-galactosidase. $\mathbf{LnL_2}$ complexes are the end product of the enzymatic cleavage of $\mathbf{LnL_1}$.

In order to test this concept, we synthesized and investigated $Gd^{3+}$, $Yb^{3+}$, and $Tb^{3+}$ complexes of $\mathbf{H_3L_1}$ and $\mathbf{H_3L_2}$ (Scheme 1, Supporting Information). Synthesis of $\mathbf{H_3L_1}$ was achieved in eight steps with a 13% overall yield starting from commercially available 2-bromo-6-amino pyridine. $\mathbf{LnL_1}$ complexes were formed at room temperature in a pH-controlled aqueous solution upon addition of the corresponding $LnCl_3$ to the ligand. Their hydrogenolysis over palladium-charcoal in water led to the formation of the corresponding $\mathbf{LnL_2}$ chelates.

Absorption spectra of the ligands $\mathbf{H_3L_1}$ and $\mathbf{H_3L_2}$ (Figure 1) display broad bands in the UV range centered at 232, 279, and

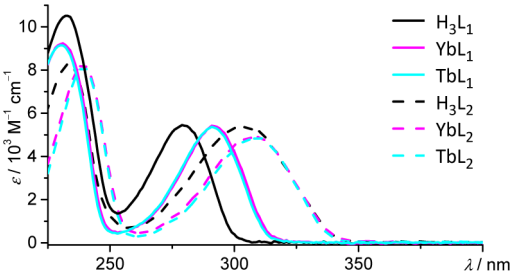


**Figure 1.** Absorption spectra of $\mathbf{H_3L_1}$ and $\mathbf{H_3L_2}$ and their corresponding $Yb^{3+}$ and $Tb^{3+}$ complexes (100 $\mu$M in HEPES buffer, pH 7.4, room temperature).

234, and 303 nm, respectively, due to $\pi \rightarrow \pi^*$ transitions. Upon formation of the $Tb^{3+}$ or $Yb^{3+}$ complexes, the low-energy absorption bands undergo a bathochromic shift of 5−10 nm. It is important to note a pronounced red-shift (25 nm, i.e., 320 vs 345 nm) of the cutoff wavelengths of the absorption bands upon conversion of $\mathbf{LnL_1}$ to $\mathbf{LnL_2}$, which can be used to our advantage in the design of responsive probes.

Excitation spectra recorded upon monitoring of the main transitions of $Tb^{3+}$ and $Yb^{3+}$ ions at 545 and 980 nm, respectively, match the shapes of the absorption ones, indicating that the sensitization of $Ln^{3+}$ ions is occurring through the organic ligands (Figure 2, left). Upon excitation into ligand-centered absorption bands at 290−310 nm, **TbL** and **YbL** complexes exhibit characteristic emission in the visible or the NIR range due to

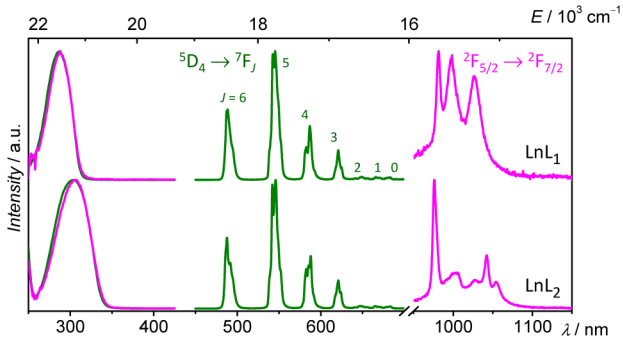


**Figure 2.** Left: excitation spectra of $\mathbf{LnL_1}$ (top) and $\mathbf{LnL_2}$ (bottom) ($\lambda_{em}$ = 545 nm ($Tb^{3+}$) and 980 nm ($Yb^{3+}$)). Center and right: emission spectra of $\mathbf{LnL_1}$ (top, $\lambda_{ex}$ = 290 nm) and $\mathbf{LnL_2}$ (bottom, $\lambda_{ex}$ = 310 nm); 100 $\mu$M in HEPES buffer, pH 7.4, room temperature. Ln = $Tb^{3+}$ (green traces), $Yb^{3+}$ (magenta traces).

$^5D_4 \rightarrow {}^7F_J$ ($J$ = 6−0) or $^2F_{5/2} \rightarrow {}^2F_{7/2}$ transitions, respectively (Figure 2, center and right). The differences in Stark splitting of the f−f transitions, which are more pronounced in the case of $Yb^{3+}$ complexes, reflect changes in coordination environment around the $Ln^{3+}$ ion.

Luminescence lifetimes and quantum yields have been determined in $H_2O$ and $D_2O$ solutions (Table S1). In $H_2O$, quantum yields and luminescence lifetime values of $\mathbf{TbL_1}$ are larger than those observed for $\mathbf{TbL_2}$ (37(1) vs 22.2(2)% and 2.78(1) vs 1.94(4) ms) but are similar when placed in $D_2O$ (∼36% and 3 ms), reflecting the role of O−H vibrations in the latter complex. Indeed, comparison of $\tau_{obs}$ in $H_2O$ and $D_2O$ using phenomenological equations[20] confirms that the $Tb^{3+}$ ion is monohydrated in $\mathbf{TbL_2}$, while no water molecule is coordinated to $Tb^{3+}$ in $\mathbf{TbL_1}$. For $Yb^{3+}$ complexes, the situation is different due to the intrinsically higher impact of vibrations on the nonradiative quenching of luminescence.[13,21] Quantum yield and lifetime values are lower even in $D_2O$ by 1.4−1.5 times for $\mathbf{YbL_2}$ compared to $\mathbf{YbL_1}$ (0.181(6) vs 0.261(5)% and 5.02(2) vs 7.7(2) $\mu$s). This result can be explained by a stronger nonradiative quenching contribution of N−H vibrations in $\mathbf{YbL_2}$. Moreover, in $H_2O$, $\mathbf{YbL_2}$ exhibits a biexponential luminescence decay with lifetimes of 1.44 and 0.77 $\mu$s. We can hypothesize the presence of an equilibrium between mono- and nonhydrated species in this case.

To analyze the abilities of the $Tb^{3+}$ and $Yb^{3+}$ complexes to operate as luminescence responsive probes upon elimination of the benzyl carbamate spacer, emission spectra of $\mathbf{LnL_1}$ and $\mathbf{LnL_2}$ were measured under ligand excitation at 340 nm (Figure 3). The choice of the excitation wavelength was dictated by the differences in absorption for the two series of complexes (Figure 1). The integrated emission intensities of $\mathbf{TbL_2}$ and $\mathbf{YbL_2}$ were found to be 20- and 6.5-times higher, respectively, than that of the corresponding $\mathbf{LnL_1}$ complexes. Thus, conversion of visible ($Tb^{3+}$) or NIR ($Yb^{3+}$) emitting probes bearing the enzyme-specific substrate to $\mathbf{LnL_2}$ complexes will lead to a turn-on luminescence response, which will be the first example of a NIR-emitting $Ln^{3+}$ complex for monitoring enzymatic reactions.

To assess the potentiality of the $Gd^{3+}$ analogues as enzyme responsive $T_1$-MRI agents, longitudinal water proton relaxivities, $r_1$, were determined for $\mathbf{GdL_1}$ and $\mathbf{GdL_2}$ (0−80 MHz, 25 and 37 °C). At all fields and both temperatures, the $r_1$ values are considerably (90−100%) larger for $\mathbf{GdL_2}$ than for $\mathbf{GdL_1}$ (Supporting Information; $r_1$ = 1.91 and 3.77 $mM^{-1}$ $s^{-1}$ for $\mathbf{GdL_1}$ and $\mathbf{GdL_2}$, respectively; 60 MHz, 25 °C). This relaxivity


DOI: 10.1021/jacs.5b12084
J. Am. Chem. Soc. 2016, 138, 2913−2916

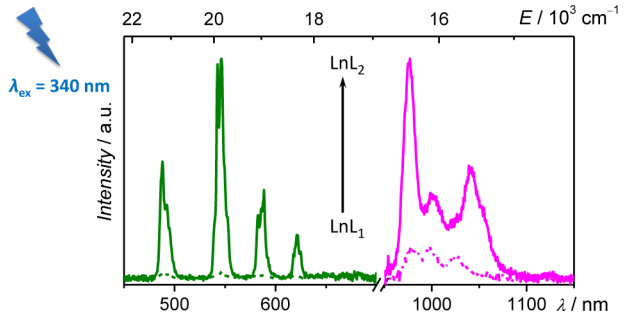


**Figure 3.** Demonstration of off−on luminescence switch from $\mathbf{LnL_1}$ (dotted line) to $\mathbf{LnL_2}$ (plain line) under excitation at 340 nm (100 $\mu$M in HEPES buffer, pH 7.4, room temperature). Ln = $Tb^{3+}$ (green traces), $Yb^{3+}$ (magenta traces).

difference should lead to a remarkable turn-on response in $T_1$-MRI upon enzymatic activation of the probe. The low relaxivity of $\mathbf{GdL_1}$ points to a nonhydrated state, in accordance with the crystal structure (Figure S8) and the luminescence lifetimes (see above), while the higher relaxivity of $\mathbf{GdL_2}$ is consistent with a monohydration of the $Ln^{3+}$.

CEST spectra were recorded for $\mathbf{TbL_1}$, $\mathbf{TbL_2}$ and $\mathbf{YbL_1}$, $\mathbf{YbL_2}$ complexes in aqueous solution by applying a 3 s selective saturation at 25 $\mu$T in 1 ppm increments from −90 to +90 ppm ($Yb^{3+}$) or −500 to +400 ppm ($Tb^{3+}$) and plotted as normalized water signal intensity ($M_z/M_0$ %) against frequency offset (ppm). A single CEST effect (~25%) was observed at +44 ppm for $\mathbf{YbL_1}$, while two CEST peaks appear at −105 and −115 ppm for $\mathbf{TbL_1}$ (Figure S2), which were assigned to carbamate protons. While amide protons are a common source of PARACEST in $Ln^{3+}$ complexes, this is the first example of carbamate protons that generate PARACEST effect. In contrast, no CEST is produced by $\mathbf{LnL_2}$ analogues (Figures 4 and S2). Thus, the conversion of

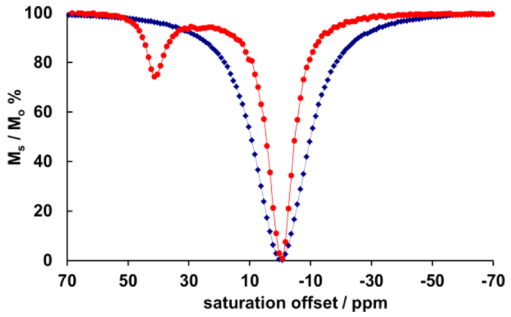


**Figure 4.** CEST spectra of $\mathbf{YbL_1}$ (red) and $\mathbf{YbL_2}$ (blue); 500 MHz, pH 7.5, 37 °C, irradiation power 25 $\mu$T, saturation time 3 s, $[\mathbf{YbLi}]_{i=1,2}$ = 20 mM.

the carbamate complexes to the amine analogues upon enzymatic reaction will lead to a turn-off PARACEST response. For $\mathbf{TbL_1}$, the two CEST peaks likely belong to two isomers, as it was reported for YbHPDO3A.[22] Indeed, $Ln^{3+}$ complexes of cyclen-based ligands may exist as two diastereomeric pairs,[23] which are observable in the $^1$H NMR spectrum of $\mathbf{TbL_1}$ (Figure S23). The two CEST signals belonging to the same molecule can be later exploited for a ratiometric calibration that reports on enzyme activities irrespective of probe concentration.

The exchange rate of the mobile carbamate protons has been assessed by QUEST measurements for $\mathbf{YbL_1}$ ($k_{ex}$ = 6100 ± 100 $s^{-1}$) and by the omega plot method for the two isomers of $\mathbf{TbL_1}$ ($k_{ex}$ = 4300 ± 300 $s^{-1}$ at −115 ppm and 5000 ± 400 $s^{-1}$ at −105 ppm; pH 7.4, 25 °C). They are similar or slightly higher compared to values reported for $Ln^{3+}$ tetraamide DOTA-derivatives with PARACEST effect.[24]

To further demonstrate the utility of our platform system, we have acquired $T_1$-weighted and CEST MR images of the $Gd^{3+}$ and $Yb^{3+}$ complexes, respectively (Figure 5). These images are in

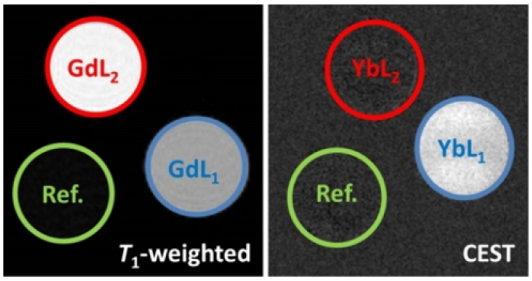


**Figure 5.** $T_1$-weighted and CEST MR images of phantoms containing complexes of $\mathbf{H_3L_1}$ and $\mathbf{H_3L_2}$ with $Gd^{3+}$ (2.86 mM, pH 7.8) and $Yb^{3+}$ (20.8 mM; pH 7.0). $T_1$-weighted images were acquired at 7 T using spin echo sequence with TE = 11.0 ms and TR = 200 ms. CEST difference images were obtained by subtracting on-resonance (+44 ppm) from off-resonance (−44 ppm) images at 9.4 T (irradiating pulse of 25 $\mu$T, 4 s).

accordance with the relaxivities of $\mathbf{GdL_1}$ and $\mathbf{GdL_2}$ and with the CEST effect observed for $\mathbf{YbL_1}$. They evidence the potential of obtaining MRI detectable responses upon the transformation of the carbamate to the corresponding amine derivative complexes, representing off−on or on−off responses in $T_1$- or CEST-MRI, respectively.

In conclusion, we have designed, synthesized and characterized the physicochemical properties of complexes formed with a ligand system that can be tuned for specific detection of a wide variety of enzymatic activities using complementary detection modalities including visible and NIR optical imaging and $T_1$- or PARACEST-MRI depending on the nature of the $Ln^{3+}$ ion. A common triggering molecular mechanism is used for the operation of different imaging modalities. $\mathbf{LnL_1}$ and $\mathbf{LnL_2}$ complexes described here model the states prior- and postenzymatic cleavage occurring in these probes.

This is the first example where a single molecular system can be used as a responsive imaging agent in three different independent modalities. In these compounds, we have evidenced a remarkable variation in relaxivity ($Gd^{3+}$), in PARACEST as well as in luminescence properties ($Tb^{3+}$ and $Yb^{3+}$), which open the way toward multimodal enzyme detection by using a single ligand.

## ■ ASSOCIATED CONTENT

### Ⓢ Supporting Information

The Supporting Information is available free of charge on the ACS Publications website at DOI: 10.1021/jacs.5b12084.

Synthetic procedures, compounds characterization, $^1$H NMR, NMRD, CEST spectra, photophysical measurements, ORTEP plot, and HPLC analyses (PDF)
Crystallographic information (CIF)

## ■ AUTHOR INFORMATION

### Corresponding Authors

*philippe.durand@cnrs.fr
*eva.jakabtoth@cnrs.fr
*stephane.petoud@inserm.fr



DOI: 10.1021/jacs.5b12084
J. Am. Chem. Soc. 2016, 138, 2913−2916

### Notes

The authors declare no competing financial interest.

## ■ ACKNOWLEDGMENTS

This research was supported by ANR (ENZYMAGE), La Ligue Contre le Cancer and carried out within European COST actions TD1004 and CM1006, and Cancéropôle Grand Ouest. S.P. acknowledges support from INSERM and J.H. acknowledges the French research ministry for her grant.

## ■ REFERENCES

(1) (a) Jung, K.-H.; Lee, K.-H. *J. Pathol. Transl. Med.* **2015**, *49*, 5. (b) Hussain, T.; Nguyen, Q. T. *Adv. Drug Delivery Rev.* **2014**, *66*, 90. (c) *Molecular Imaging: Principles and Practice*; Weissleder, R.; Ross, B. D.; Rehemtulla, A.; Gambhir, S. S., Eds.; People's Medical Publishing House: Shelton, 2010.

(2) *The Chemistry of Molecular Imaging*; Long, N. J.; Wong, W.-T., Eds.; Wiley: New York, 2015.

(3) (a) Hingorani, D. V.; Bernstein, A. S.; Pagel, M. D. *Contrast Media Mol. Imaging* **2015**, *10*, 245. (b) Boros, E.; Gale, E. M.; Caravan, P. *Dalton Trans.* **2015**, *44*, 4804. (c) Bonnet, C. S.; Tei, L.; Botta, M.; Toth, E. In *Chemistry of Contrast Agents in Medical Magnetic Resonance Imaging*, 2nd ed.; Merbach, A., Helm, L., Tóth, É., Eds.; John Wiley & Sons Ltd., 2013; p 343. (d) Terreno, E.; Castelli, D. D.; Aime, S. In *Chemistry of Contrast Agents in Medical Magnetic Resonance Imaging*, 2nd ed.; Merbach, A., Helm, L., Tóth, É., Eds.; John Wiley & Sons Ltd., 2013; p 387.

(4) (a) Lou, Z.; Li, P.; Han, K. *Acc. Chem. Res.* **2015**, *48*, 1358. (b) Kobayashi, H.; Choyke, P. L. *Acc. Chem. Res.* **2011**, *44*, 83.

(5) van Rooij, T.; Daeichin, V.; Skachkov, I.; de Jong, N.; Kooiman, K. *Int. J. Hyperthermia* **2015**, *31*, 90.

(6) Van de Bittner, G. C.; Ricq, E. L.; Hooker, J. M. *Acc. Chem. Res.* **2014**, *47*, 3127.

(7) (a) Seibold, U.; Wängler, B.; Schirrmacher, R.; Wängler, C. *BioMed Res. Int.* **2014**, *2014*, 13 (Article ID 153741). (b) Chiang, S. *Frontiers in Neurology* **2015**, *6*, 74. (c) Kobayashi, H.; Longmire, M. R.; Ogawa, M.; Choyke, P. L. *Chem. Soc. Rev.* **2011**, *40*, 4626.

(8) (a) Srivastava, A. K.; Kadayakkara, D. K.; Bar-Shir, A.; Gilad, A. A.; McMahon, M. T.; Bulte, J. W. M. *Dis. Models & Mech.* **2015**, *8*, 323. (b) Hingorani, D. V.; Yoo, B.; Bernstein, A. S.; Pagel, M. D. *Chem. - Eur. J.* **2014**, *20*, 9840. (c) Razgulin, A.; Ma, N.; Rao, J. *Chem. Soc. Rev.* **2011**, *40*, 4186.

(9) (a) Reilly, R. M.; Lam, K.; Chan, C.; Levine, M. *Bioconjugate Chem.* **2015**, *26*, 625. (b) Pierre, V.; Allen, M.; Caravan, P. *JBIC, J. Biol. Inorg. Chem.* **2014**, *19*, 127. (c) Heffern, M. C.; Matosziuk, L. M.; Meade, T. J. *Chem. Rev.* **2014**, *114*, 4496. (d) Wolfbeis, O. S. *Angew. Chem., Int. Ed.* **2013**, *52*, 9864.

(10) (a) Chen, K.; Chen, X. Y. *Curr. Top. Med. Chem.* **2010**, *10*, 1227. (b) Pershagen, E.; Borbas, K. E. *Angew. Chem., Int. Ed.* **2015**, *54*, 1787.

(11) Chauvin, T.; Durand, P.; Bernier, M.; Meudal, H.; Doan, B. T.; Noury, F.; Badet, B.; Beloeil, J. C.; Toth, E. *Angew. Chem., Int. Ed.* **2008**, *47*, 4370.

(12) Smith, A. M.; Mancini, M. C.; Nie, S. *Nat. Nanotechnol.* **2009**, *4*, 710.

(13) Comby, S.; Bünzli, J.-C. G. In *Handbook on the Physics and Chemistry of Rare Earths*; Gschneidner, K. A., Jr., Bünzli, J.-C. G., Pecharsky, V. K., Eds.; Elsevier Science B.V.: Amsterdam, 2007; Vol. *37*, Ch. 235, p 217.

(14) (a) Foucault-Collet, A.; Shade, C. M.; Nazarenko, I.; Petoud, S.; Eliseeva, S. V. *Angew. Chem., Int. Ed.* **2014**, *53*, 2927. (b) Foucault-Collet, A.; Gogick, K. A.; White, K. A.; Villette, S.; Pallier, A.; Collet, G.; Kieda, C.; Li, T.; Geib, S. J.; Rosi, N. L.; Petoud, S. *Proc. Natl. Acad. Sci. U. S. A.* **2013**, *110*, 17199.

(15) (a) Bünzli, J.-C. G.; Eliseeva, S. V. In *Comprehensive Inorganic Chemistry II*; Yam, V. W.-W., Ed.; Elsevier B.V.: Amsterdam, 2013; Vol. *8*, p 339. (b) Trivedi, E. R.; Eliseeva, S. V.; Jankolovits, J.; Olmstead, M. M.; Petoud, S.; Pecoraro, V. L. *J. Am. Chem. Soc.* **2014**, *136*, 1526.

(16) Amoroso, A. J.; Pope, S. J. A. *Chem. Soc. Rev.* **2015**, *44*, 4723.

(17) Hancock, R. D. *Chem. Soc. Rev.* **2013**, *42*, 1500.

(18) (a) de Bettencourt-Dias, A.; Barber, P. S.; Viswanathan, S. *Coord. Chem. Rev.* **2014**, *273−274*, 165. (b) Uh, H.; Petoud, S. *C. R. Chim.* **2010**, *13*, 668.

(19) Alouane, A.; Labruère, R.; Le Saux, T.; Schmidt, F.; Jullien, L. *Angew. Chem., Int. Ed.* **2015**, *54*, 7492.

(20) Beeby, A.; Clarkson, I. M.; Dickins, R. S.; Faulkner, S.; Parker, D.; Royle, L.; de Sousa, A. S.; Williams, J. A. G.; Woods, M. *J. Chem. Soc., Perkin Trans. 2* **1999**, 493.

(21) Bünzli, J.-C. G.; Eliseeva, S. V. *J. Rare Earths* **2010**, *28*, 824.

(22) Delli Castelli, D.; Terreno, E.; Aime, S. *Angew. Chem., Int. Ed.* **2011**, *50*, 1798.

(23) Platas-Iglesias, C. *Eur. J. Inorg. Chem.* **2012**, 2023.

(24) Zhang, S. R.; Michaudet, L.; Burgess, S.; Sherry, A. D. *Angew. Chem., Int. Ed.* **2002**, *41*, 1919.



DOI: 10.1021/jacs.5b12084
*J. Am. Chem. Soc.* 2016, 138, 2913−2916